Pharmaceutical Research, Vol. 24, No. 6, June 2007 (© 2007)
DOI: 10.1007/s11095-007-9264-x

Research Paper

FDG-PET for Pharmacodynamic Assessment of the Fatty Acid Synthase Inhibitor C75 in an Experimental Model of Lung Cancer

Jae Sung Lee,[1,4] Hajime Orita,[2] Kathleen Gabrielson,[3] Sara Alvey,[3] Ruth L. Hagemann,[1] Francis P. Kuhajda,[2] Edward Gabrielson,[2] and Martin G. Pomper[1,5]

Received November 16, 2006; accepted January 2, 2007; published online April 3, 2007

Purpose. Fatty acid synthase (FAS) is an emerging target for anticancer therapy with a variety of new FAS inhibitors being explored in preclinical models. The aim of this study was to use positron emission tomography with [^{18}F]fluorodeoxyglucose (FDG-PET) to monitor the effects of the FAS inhibitor C75 on tumor glucose metabolism in a rodent model of human A549 lung cancer.
Materials and Methods. After a baseline FDG-PET scan, C75 was administered and post-treatment scans were performed serially. FAS activity was measured in treated animals *ex vivo* by [^{14}C]acetate incorporation in animals euthanized in parallel to those imaged.
Results. Longitudinally measured metabolic volumes of interest and tumor/background ratios demonstrated a transient, reversible decrease in glucose metabolism and tumor metabolic volume after treatment, with the peak effect seen at 4 h. FDG-PET measurements correlated with changes in tumor FAS activity measured *ex vivo*.
Conclusions. Because C75 causes an effect that is shorter in duration than expected, modification of the current weekly dosing regimen should be considered. These results demonstrate the utility of small animal FDG-PET in assessing the pharmacodynamics of new anticancer agents in preclinical models.

KEY WORDS: α-methylene-γ-butyrolactone; enzyme inhibitor; fluorodeoxyglucose; positron emission tomography; small animal imaging.

INTRODUCTION

Fatty acid synthase (FAS, EC 2.3.1.85) is a multifunctional enzymatic complex that catalyzes the formation of palmitate from acetyl-coenzyme A and malonyl-coenzyme A (1). It is expressed at high levels in a wide variety of cancers (2,3). Although the exact role of overexpressed FAS in the neoplastic phenotype is not fully understood, this enzyme is emerging as a promising target for anticancer therapy (4), and efforts are underway to synthesize selective, nontoxic inhibitors of FAS (3,5). The α-methylene-γ-butyrolactone C75 is a prototypic FAS inhibitor that has demonstrated effect against tumor cells both *in vitro* and in a rodent model of mesothelioma (5,6). While we have found that treating animals with C75 does not result in injury to normal tissues, dose-limiting toxicity is due to its severe anorectic effects, necessitating a once weekly dosing regimen in our experimental studies. We hypothesize that carnitine palmitoyltransferase-1 (CPT-1) stimulation signals a positive energy balance that results in the perception of satiety (7,8). In order to extend the use of C75 and other selective FAS inhibitors to other experimental tumor models *in vivo*, we sought to understand better the pharmacodynamics of C75 *in vivo* in an orthotopic lung xenograft model in rats. The goal was to determine if the weekly dosing schedule would be sufficient to provide an objective antitumor effect measured both by changes in glucose metabolism as well as by changes in metabolic tumor volume, i.e., the volume of FDG-avid tumor, rather than by survival studies or sacrifice and necropsy of multiple animals at several time points.

To study the pharmacodynamics of C75, we employed positron emission tomography with [^{18}F]fluorodeoxyglucose (FDG-PET) in orthotopically transplanted A549 lung tumors at various times up to 1 week after initiation of treatment with C75. In parallel to rats that were imaged, rats treated in a similar manner were sacrificed at corresponding time points to measure FAS activity by traditional methods. Together, these studies provide the first noninvasive evaluation of the pharmacodynamics of a FAS inhibitor, with validation of the technique by *ex vivo* FAS analysis. By performing repeat imaging in the same animals we have been able to determine

Jae Sung Lee and Hajime Orita contributed equally to this work

[1] Department of Radiology, Johns Hopkins Medical Institutions, 1550 Orleans Street, 492 CRB II, Baltimore, Maryland 21231, USA.
[2] Department of Pathology, Johns Hopkins Medical Institutions, Baltimore, Maryland 21231, USA.
[3] Department of Molecular and Comparative Pathobiology, Johns Hopkins Medical Institutions, Baltimore, Maryland 21231, USA.
[4] Present Address: Seoul National University College of Medicine, Seoul, 110-744, South Korea
[5] To whom correspondence should be addressed. (e-mail: mpomper@jhmi.edu.)

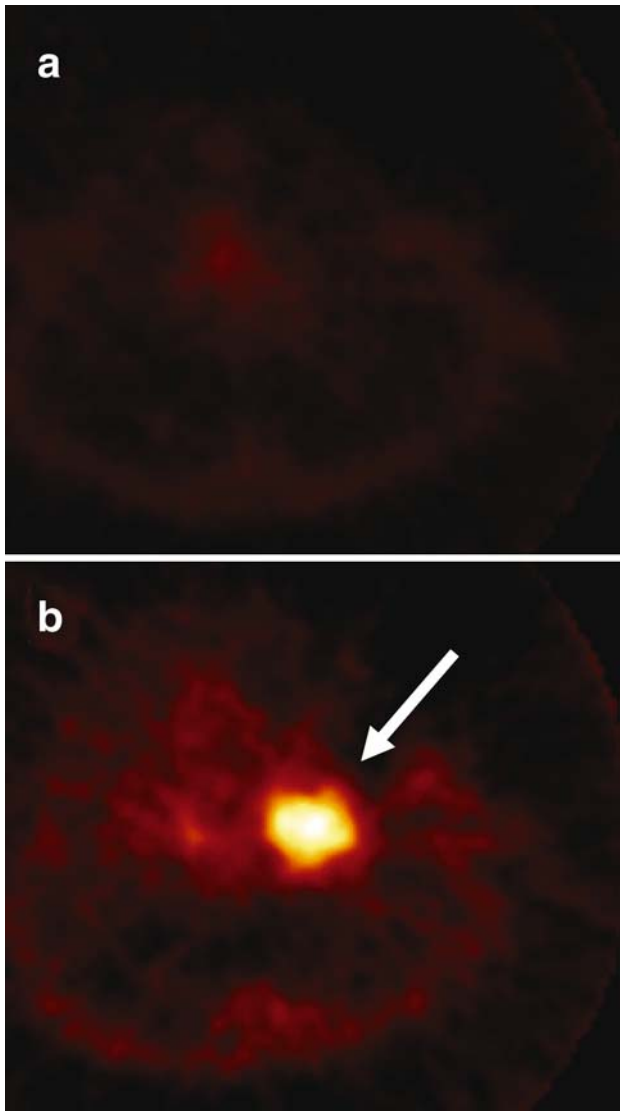

Fig. 1. Repeated baseline transaxial FDG-PET images obtained to monitor the growth of A549 human lung cancer orthotopic xenografts in nude rats. (**a**) At 3 weeks after tumor cell implantation there is little radiopharmaceutical uptake within lungs. (**b**) Markedly increased FDG uptake in the tumor mass at 4 weeks after tumor implantation (*arrow*).

that C75 provides only a transient and reversible growth inhibition in this lung cancer model, suggesting that alternative dosing regimens with this compound or compounds of this class may be necessary.

MATERIALS AND METHODS

Lung Cancer Xenograft Model

All animal experiments were done in accordance with guidelines on animal care and use established by the Johns Hopkins University School of Medicine Institutional Animal Care and Use Committee. The A549 human lung cancer cell line was obtained from ATCC (Manassas, VA) and cultured using recommended conditions. For establishing orthotopic xenografts, athymic nude male rats (National Cancer Institute, Frederick, MD) weighing 200–220 g were irradiated 1 day prior to tumor cell implantation, using a Cesium 137 AECL Gamma cell 40 irradiator (Nordion, Ottowa, Ontario, Canada), for a total of 55R per animal (9). Animals were anesthetized with 75 mg/kg ketamine and 10 mg/kg xylazine administered by intraperitoneal injection, placed head up in a dorsal recumbent position (45° incline), and inoculated with 10 million cells, suspended in RPMI1640 medium with 1 mM EDTA, into the trachea using transdermal laryngotracheal illumination and modified 16-gauge intravenous catheters. After inoculation, animals were maintained on a standard diet for 3 weeks to allow tumor growth.

Fatty Acid Synthesis Inhibitor

C75, a slow-binding inhibitor of mammalian FAS, was provided by FASgen, Inc. (Baltimore, MD), dissolved in RPMI media (5 mg/mL), and filter sterilized prior to use.

Small Animal PET Imaging

For imaging the rats with lung cancer xenografts, we used a dedicated small animal PET scanner (Advanced Technology Laboratory Animal Scanner: ATLAS) with an 11.8 cm diameter aperture and a 2 cm axial field-of-view (FOV). ATLAS is a dual-layer phoswich PET scanner developed at the National Institutes of Health (Bethesda, MD), which has the capability of measurement of depth interaction (DOI) information (10). LGSO-GSO phoswich crystal elements in this scanner provide a two-level estimate of the depth at which an annihilation photon is absorbed in the phoswich crystal element, either in the LGSO (light decay time = 40 ns) portion of the element or in the GSO (light decay time = 60 ns) portion. Knowledge of this depth substantially reduces the parallax error while preserving sensitivity compared to other scanners of similar ring

Table I. Changes in Body Weights and PET Parameters

	Baseline	4 h	24 h	48 h	1 week
Weight (g)	249 ± 38	248 ± 38	229 ± 36*	224 ± 31*	234 ± 37*
Maximum T/B	6.20 ± 0.82	4.60 ± 0.77**	5.42 ± 1.55	5.63 ± 0.76	6.62 ± 1.25
Mean T/B	3.87 ± 0.16	3.41 ± 0.47	3.70 ± 0.39	3.81 ± 0.19	4.15 ± 0.40
Tumor metabolic volume (mL)	1.88 ± 0.17	1.06 ± 0.31**	1.21 ± 0.57	1.59 ± 0.51	2.02 ± 0.67
(Max T/B) × volume (m)	11.74 ± 2.20	4.77 ± 1.30***	9.26 ± 5.30	7.86 ± 4.31	14.10 ± 6.34
(Mean T/B) × volume (m)	7.30 ± 0.89	3.51 ± 0.76‡	5.56 ± 2.66	5.30 ± 2.30	8.60 ± 3.35

*$P < 0.05$ vs. baseline
**$P < 0.005$ vs. baseline
***$P < 0.0005$ vs. baseline
values are shown as mean ± SD

diameter without this capability (11). The spatial resolution of the reconstructed FDG-PET image was 1.8 mm (radial and tangential) using a 2D FBP (filtered back projection) (12,13). Peak sensitivity at the center of the axial FOV was > 2.0% after correcting for positron escape from the source (100–700 keV energy window) (13,14). For quality control of the scanner, a microcylindrical uniform phantom filled with 24 mL water and ~300 μCi of FDG was scanned before or after the animal experiments. Uniformity of count distribution across the FOV and consistency in counting efficiency were checked daily.

Rats were fasted overnight prior to imaging on the next morning. Animals were anesthetized by intraperitoneal administration of a cocktail containing ketamine (90 mg/kg) and xylazine (10 mg/kg), and baseline FDG-PET scans were performed after injecting 450 MBq/kg of FDG in a volume of ~ 0.2 mL into the jugular vein. For this procedure, each anesthetized rat was placed in the supine position on the ATLAS imaging bed, centering the lung in the transaxial FOV. One hour whole-body PET scans (20 min per bed position; three bed positions) were performed 20 min after the radiotracer injection using the ATLAS PET scanner. The rats were automatically advanced in three steps through the scanning aperture to acquire partially overlapping data sets (number of overlap = 4 slices) spanning from the shoulder to the middle of the liver. Fully 3-dimensional frame mode data were acquired with an open energy window (100–700 keV) and an effective time window of 5 ns. PET images were corrected for decay and reconstructed using 2D FBP algorithm. Image data were not corrected for attenuation or scatter. Image pixel size was 0.56 mm transaxially with a 1.13-mm slice thickness.

FDG-PET scans were repeatedly performed on four rats beginning at 3 weeks after tumor cell implantation at an interval of 1 week to monitor tumor growth. If the visible mass in the lung was detected in that baseline PET image, animals were treated one time with C75 (20 mg/kg IP) and additional scans were performed at designated time intervals (4, 24, and 48 h and 1 week) using the same procedures outlined above.

Image Analysis

Tumor/background ratio (T/B) and tumor volume were determined on each PET image for semiquantitative analysis of the effects of C75 treatment. To measure the background activity, volumes of interest (VOIs) were manually drawn over subcutaneous soft tissue through multiple slices. A sufficiently large area was included in the background region to minimize the effects of VOI delineation on the T/B calculation. On average, the number of voxels in the background VOI was 3,630 (= 1.29 cc). To determine the tumor VOIs objectively, we used a two-step approach. Initial tumor VOIs were drawn manually over the tumor mass on the baseline PET images acquired a day before the C75 administration and an average T/B ratio in each image was determined. The mean (μ) and standard deviation (SD) of the average T/B ratio were calculated and $\mu - 2 \times SD$ value ($= 3.97 - 2 \times 0.47 \approx 3.0$) was determined as the threshold for the T/B ratio in the next step. In the second step, a large VOI that included all lung lobes and the trachea but excluded the heart, bone marrow, and injection site (jugular vein) was drawn on each PET image. Those VOIs were used to define the mask area in which the final tumor regions were automatically determined using the threshold T/B = 3.0 obtained in the previous step. This two-step approach was devised to define the tumor regions in all the images with the

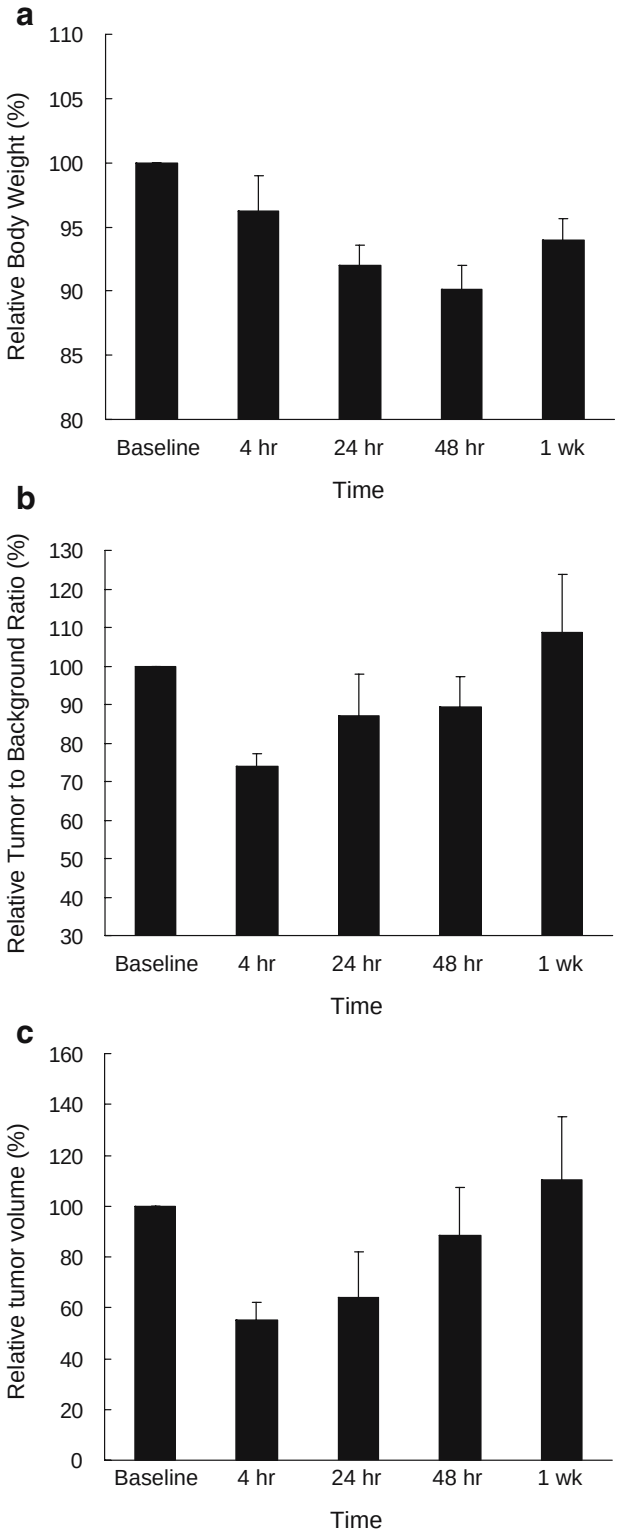

Fig. 2. Change in animal body weight (**a**), maximum tumor to background ratio (T/B) (**b**), and tumor metabolic volume (**c**) compared to the values measured in the baseline PET scan in four tumor-bearing rats treated with C75. Data are presented as mean percentage change ± SEM.

same criteria, T/B > 3.0. Numbers of voxels within the tumor in the final tumor images were converted into the metabolic tumor volume (in mL). Averages of the 100 highest voxel values and all voxel values in the tumor regions in each image were normalized to the mean background value to calculate the maximum and mean T/B ratios, respectively. A single maximal voxel value was not used to calculate the maximum T/B ratio since such analysis was fraught with unacceptable levels of statistical noise.

FAS Enzymatic Activity

FAS enzymatic activity was measured in tissues removed from animals treated in parallel with those imaged, and sacrificed at time intervals after treatment corresponding to the times used for PET imaging. In brief, lung tumors and liver tissue samples were removed immediately after sacrifice, pulverized on ice, and used as extract for measurement of [^{14}C]acetate incorporation into total lipids, as previously described (2). Three animals were used for each time point, and three samples (each for liver and lung tumor) were obtained from each animal. Because the variance in measurements across animals was similar to that across samples taken from individual animals, all nine samples for each time point were used to calculate means and standard deviations for the respective time points. Results were compared to control (untreated animals) for t-test measure of significance.

Statistical Analysis

Changes in body weight, maximum T/B, mean T/B, tumor metabolic volume, (maximum T/B) × metabolic volume, and (mean T/B) × metabolic volume were evaluated using repeated measures analysis of variance (ANOVA), with time as the repeated factor. P values less than 0.05 were considered statistically significant.

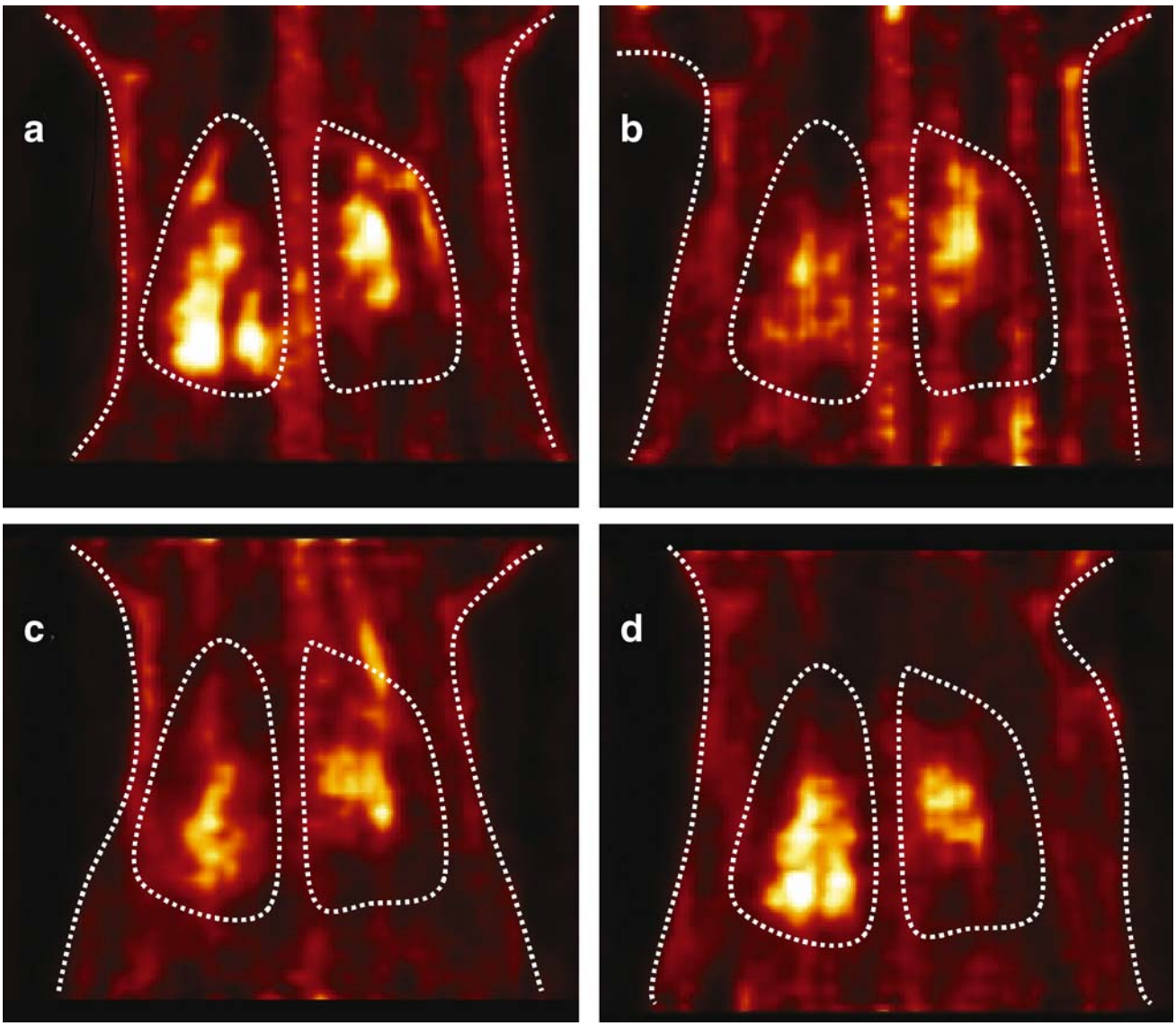

Fig. 3. Serial, coronal FDG-PET images of a representative tumor-bearing rat treated with C75. (**a**) Baseline (1 day before C75 treatment). (**b**) 4 hours after treatment. (**c**) 24 hours after treatment. (**d**) 1 week after treatment.

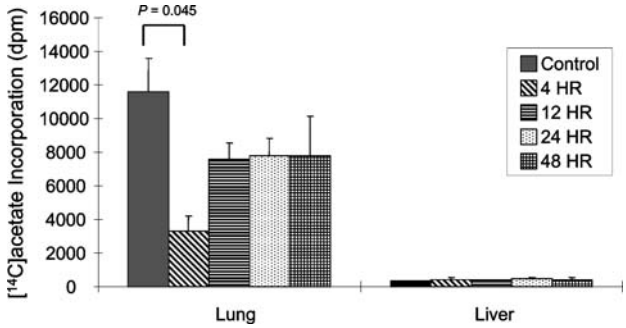

Fig. 4. *Ex vivo* FAS activity assay. The 4-hour time point shows significantly diminished [^{14}C]acetate incorporation, indicating decreased FAS activity. That result corresponds to the decreased FDG uptake also noted only at the 4-hour time point (Fig. 4).

RESULTS

Monitoring Tumor Growth by PET Imaging

Baseline (pretreatment) FDG-PET scanning was performed repeatedly in animals to monitor tumor growth. A transaxial PET image of a representative rat scanned three weeks after the tumor cell injection is shown in Fig. 1a. Diffuse tumor uptake of FDG observed in the lungs was slightly higher than that of the background in that instance. In the PET image of the same animal taken one week later, FDG uptake in the tumor mass was markedly increased (tumor metabolic volume = 1.6 mL; maximum T/B = 6.2) as shown in Fig. 1b.

Time-Dependent Effects of C75 on FDG Uptake

C75-induced changes in body weight and PET data are summarized in Table I. After C75 treatment, the animals lost weight that was partially recovered within a week as graphically shown in Fig. 2a. That weight loss was similar to that demonstrated in our previous studies (2,6). Relative to the weight at the time of the baseline PET scan (249 ± 44 g), the animals underwent a 9.8% decrease in weight after 48 h. On average, weight recovered to 94% of the baseline value at 1 week after treatment.

Longitudinally measured maximum T/B of FDG uptake and tumor metabolic volume are shown in Fig. 2b and c, which illustrate the transient and reversible decrease of glucose metabolism and the metabolic volume of tumor xenografts after the C75 treatment. Compared to the baseline (maximum T/B = 6.2 ± 0.82; tumor metabolic volume = 1.88 ± 0.17 mL), tumors in the animals scanned 4 h after treatment showed an acute decrease of FDG uptake (26% decrease on average and tumor metabolic volume (45% decrease). Note that the volume that is decreasing is FDG-avid, i.e., *metabolic* volume, rather than *anatomic* volume, as would be measured by computed tomography (CT) or magnetic resonance imaging (MRI). By contrast, the anatomic volume would be expected to remain invariant by this early point in time when compared to baseline. Relative to the 4 h post-treatment scan, PET scans performed at 24 h, 48 h and 1 week after treatment demonstrated increased metabolic activity of tumor after initial regression. Maximum T/B on 24 h, 48 h and one week post-treatment scans were 87, 89 and 109% of the baseline value and tumor metabolic volumes were 64, 88 and 111%, respectively. Mean T/B changed in similar pattern: mean T/B at baseline was 3.87 ± 0.16 and 88, 95, 99 and 108% of the baseline value after 4, 24 and 48 h and 1 week, respectively. The changes in the multiplication of maximum or mean T/B and tumor metabolic volume, which would reflect the total change in tumor radioactivity, were greater than 50% on the 4 h post-treatment scan (40 and 47% of the baseline, respectively). Fig. 3 shows the representative coronal FDG-PET images of a tumor-bearing rat treated with C75. The heart is not in the FOV on the images chosen.

Time-Dependent Effects of C75 on FAS Enzymatic Activity

Using [^{14}C]acetate incorporation into total lipids as a measure of drug effect on FAS activity, C75 treatment was noted to result in a significant inhibition of FAS that appeared to be maximal at 4 h after treatment (Fig. 4). That activity increased over the following 44 h, similar to the increase in FDG uptake observed in the PET imaging studies.

DISCUSSION

PET imaging has matured into an important method to follow anticancer therapy serially and noninvasively in the clinical setting (15). Because it measures functional or metabolic phenomena, i.e., represents a clinical derivative of molecular imaging, the changes detected by PET will occur sooner than those detected by the traditional imaging methods of CT or MRI, which are anatomically based. PET has demonstrated the ability to predict the response to chemotherapy within several days of initiating treatment and is being used increasingly to hasten new drug development (16–19).

In this study we used FDG-PET imaging in a preclinical model of lung cancer to determine the pharmacodynamics of C75, an inhibitor of FAS. Fatty acid biosynthesis is a minor pathway by which cells, particularly malignant cells, accumulate energy (20). This system acts largely in parallel to another mechanism for energy accumulation, involving GLUT-1, which facilitates intracytoplasmic transport of glucose, and is directly related to FDG uptake in tumors,

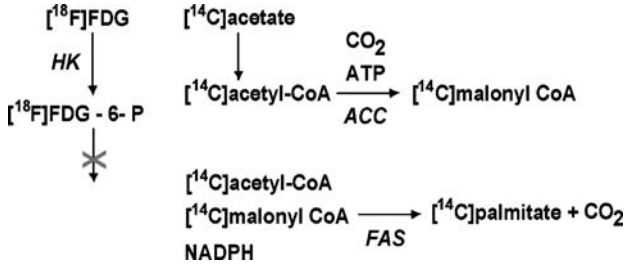

Fig. 5. Fate of [^{18}F]fluorodeoxyglucose ([^{18}F]FDG) and [^{14}C]acetate in the cancer cell. [^{18}F]FDG is actively transported into the cell and is phosphorylated by hexokinase (HK), but unlike glucose, remains trapped in the cytoplasm. It cannot be further incorporated into fatty acids. In contrast, [^{14}C]acetate, among its many possible biochemical fates, is incorporated into fatty acids. [^{14}C]acetate is initially esterified to coenzyme-A (CoA) prior to entering synthetic pathways. In lipogenic cells, [^{14}C]acetyl-CoA is a substrate for acetyl-CoA carboxylase (ACC), which produces [^{14}C]malonyl-CoA. Fatty acid synthase (FAS) uses three substrates, [^{14}C]acetyl-CoA, [^{14}C]malonyl-CoA, and NADPH to produce the free fatty acid, [^{14}C]palmitate. Stoichiometrically, FAS utilizes 1 acetyl-CoA, 7 malonyl-CoA, and 7 NADPH to produce one molecule of palmitate and 7 CO_2.

including lung cancer (20,21) (Fig. 5). Although the mechanism of action of C75 may not be directly related to cellular pathways that mediate FDG uptake, the effects of inhibition of FAS eventually lead to apoptosis, which is manifested in lower overall glucose uptake in the tumor (22). We have shown that C75 has proved promising in two previous tumor models *in vivo*, and have shown in this report that it is effective in the A549 human lung cancer model (5,6). However, as an inhibitor of FAS, C75 produces dose-limiting anorexia. In fact, C75 and compounds of this class are being pursued as anti-obesity agents (8). Consequently it is important to understand the pharmacodynamics of C75 in order to optimize the antitumor treatment regimen. We validated the imaging method for assessment of pharmacodynamics of C75 by sacrificing animals that were treated in parallel and measuring FAS activity using conventional biochemical methods in tissue samples from these animals. Both approaches demonstrated that peak biochemical activity of C75 upon the tumor occurs soon after treatment (4 h). Inhibition of FAS activity and of FDG uptake both diminish over subsequent time periods, with full recovery of metabolic tumor volume by 1 week, suggesting a transient effect of C75 with one-time dosing.

These findings have several implications for developing a feasible clinical dosing regimen for C75 or, perhaps more broadly, this class of FAS inhibitors. For example, because we have shown that the duration of action of C75 is significantly less than the necessary (due to anorexia) 1 week dosing interval, it may be necessary to maintain nutritional status in these animals through appetite stimulation or force-feeding, to allow more frequent dosing of these compounds. Alternatively, this study suggests that it may be more prudent to invest in the development of a new generation of FAS inhibitors that are less likely to cause significant anorexia (3). In general, this study demonstrates one application of preclinical PET imaging to monitoring the pharmacodynamics of cancer treatment. FDG-PET may be particularly useful for therapeutic monitoring of metabolic anticancer agents such as those that target FAS.

ACKNOWLEDGMENTS

The authors appreciate the suggestions and comments of Dr. Jurgen Seidel and Michael Green of the National Institutes of Health, Clinical Center. This work was supported by grants from the National Cancer Institute (P50 CA058184, R01 CA101232 and U24 CA92871).

REFERENCES

1. R. Lupuand and J. A. Menendez. Targeting fatty acid synthase in breast and endometrial cancer: an alternative to selective estrogen receptor modulators?. *Endocrinology* **147**:4056–4066 (2006).
2. E. S. Pizer, J. Thupari, W. F. Han, M. L. Pinn, F. J. Chrest, G. L. Frehywot, C. A. Townsend, and F. P. Kuhajda. Malonyl-coenzyme-A is a potential mediator of cytotoxicity induced by fatty-acid synthase inhibition in human breast cancer cells and xenografts. *Cancer Res.* **60**:213–218 (2000).
3. J. M. McFadden, S. M. Medghalchi, J. N. Thupari, M. L. Pinn, A. Vadlamudi, K. I. Miller, F. P. Kuhajda, and C. A. Townsend. Application of a flexible synthesis of (5R)-thiolactomycin to develop new inhibitors of type I fatty acid synthase. *J. Med. Chem.* **48**:946–961 (2005).
4. F. P. Kuhajda. Fatty acid synthase and cancer: new application of an old pathway. *Cancer Res.* **66**:5977–5980 (2006).
5. F. P. Kuhajda. Fatty-acid synthase and human cancer: new perspectives on its role in tumor biology. *Nutrition* **16**:202–208 (2000).
6. E. W. Gabrielson, M. L. Pinn, J. R. Testa, and F. P. Kuhajda. Increased fatty acid synthase is a therapeutic target in mesothelioma. *Clin. Cancer Res.* **7**:153–157 (2001).
7. S. H. Cha, Z. Hu, S. Chohnan, and M. D. Lane. Inhibition of hypothalamic fatty acid synthase triggers rapid activation of fatty acid oxidation in skeletal muscle. *Proc. Natl. Acad. Sci. U. S. A.* **102**:14557–14562 (2005).
8. F. P. Kuhajda, L. E. Landree, and G. V. Ronnett. The connections between C75 and obesity drug-target pathways. *Trends Pharmacol. Sci.* **26**:541–544 (2005).
9. T. H. March, P. G. Marron-Terada, and S. A. Belinsky. Refinement of an orthotopic lung cancer model in the nude rat. *Vet. Pathol.* **38**:483–490 (2001).
10. J. Seidel, J. J. Vaquero, J. Pascau, and M. Desco. Features of the NIH atlas small animal PET scanner and its use with a coaxial small animal volume CT scanner. In *Conference Proceeding of IEEE International Symposium on Biomedical Imaging*, 2002, pp. 545–548.
11. J. Seidel, J. J. Vaquero, and M. V. Green. Resolution uniformity and sensitivity of the NIH ATLAS small animal PET scanner: comparison to simulated LSO scanners without depth-of-interaction capability. *IEEE Nucl. Sci. Symp. Conf. Rec.* **3**:1555–1558 (2001).
12. R. Yao, J. Seidel, C. A. Johnson, M. E. Daube-Witherspoon, M. V. Green, and R. E. Carson. Performance characteristics of the 3-D OSEM algorithm in the reconstruction of small animal PET images. Ordered-subsets expectation-maximixation. *IEEE Trans. Med. Imag.* **19**:798–804 (2000).
13. J. S. Lee, R. L. Hagemann, Y. Wang, B. M. Tsui, and M. G. Pomper. Performance evaluation of the NIH ATLAS II small animal PET scanner. In *Annual Meeting of Society for Molecular Imaging*, San Francisco, CA (2003).
14. J. Seidel, J. J. Vaquero, and M. V. Green. Resolution uniformity and sensitivity of the NIH ATLAS small animal PET scanner: Comparison to simulated LSO scanners without depth-of-interaction capability. *IEEE Trans. Nucl. Sci.* **50**:1347–1350 (2003).
15. M. E. Juweid and B. D. Cheson. Positron–emission tomography and assessment of cancer therapy. *N. Engl. J. Med.* **354**:496–507 (2006).
16. G. D. Demetri, M. Mehren von, C. D. Blanke, A. D. Van den Abbeele, B. Eisenberg, P. J. Roberts, M. C. Heinrich, D. A. Tuveson, S. Singer, M. Janicek, J. A. Fletcher, S. G. Silverman, S. L. Silberman, R. Capdeville, B. Kiese, B. Peng, S. Dimitrijevic, B. J. Druker, C. Corless, C. D. Fletcher, and H. Joensuu. Efficacy and safety of imatinib mesylate in advanced gastrointestinal stromal tumors. *N. Engl. J. Med.* **347**:472–480 (2002).
17. A. Saleem, N. Charnley, and P. Price. Clinical molecular imaging with positron emission tomography. *Eur. J. Cancer* **42**:1720–1727 (2006).
18. R. Weissleder. Molecular imaging in cancer. *Science* **312**:1168–1171 (2006).
19. W. A. Weber. Chaperoning drug development with PET. *J. Nucl. Med.* **47**:735–737 (2006).
20. V. Sebastiani, P. Visca, C. Botti, G. Santeusanio, G. M. Galati, V. Piccini, B. Capezzone de Joannon, U. Di Tondo, and P. L. Alo. Fatty acid synthase is a marker of increased risk of recurrence in endometrial carcinoma. *Gynecol. Oncol.* **92**:101–105 (2004).
21. M. Mamede, T. Higashi, M. Kitaichi, K. Ishizu, T. Ishimori, Y. Nakamoto, K. Yanagihara, M. Li, F. Tanaka, H. Wada, T. Manabe, and T. Saga. [18F]FDG uptake and PCNA, Glut-1, and Hexokinase-II expressions in cancers and inflammatory lesions of the lung. *Neoplasia* **7**:369–379 (2005).
22. J. N. Li, M. Gorospe, F. J. Chrest, T. S. Kumaravel, M. K. Evans, W. F. Han, and E. S. Pizer. Pharmacological inhibition of fatty acid synthase activity produces both cytostatic and cytotoxic effects modulated by p53. *Cancer Res.* **61**:1493–1499 (2001).